ELSEVIER

Chemical Engineering Journal 92 (2003) 81–90

Chemical Engineering Journal

www.elsevier.com/locate/cej

Bubble size distribution and gas–liquid mass transfer in airlift contactors

Porntip Wongsuchoto, Tawatchai Charinpanitkul, Prasert Pavasant*

Department of Chemical Engineering, Faculty of Engineering, Chulalongkorn University, Bangkok 10330, Thailand

Received 2 January 2002; accepted 18 May 2002

Abstract

This work investigated the distribution of bubble size in annulus sparged airlift contactors (ALCs). Increasing gas velocity in the ALC considerably reduced the size of the bubble and shifted the distribution of bubble size from the normal to log-normal types. Bubble size was found to decrease along the axial distance in the riser of the ALC. Moreover, an increase in the ratio between the cross-sectional areas of the downcomer and riser was found to result in the decreasing bubble size at high superficial gas velocity. Spargers with a large number of orifices led to a larger bubble size in the system. In contrast, it was found that a comparatively broad bubble size distribution was caused by employing a gas sparger with less number of orifices. This work also examined the gas–liquid mass transfer characteristics of the ALC in forms of mass transfer coefficient and specific interfacial area which were individually evaluated. It was found that the specific interfacial area, rather than the mass transfer coefficient, played a more significant role in controlling the overall rate of mass transfer in the system.

Keywords: Airlift contactor; Mass transfer; Bubble size; Bubble size distribution

1. Introduction

Gas–liquid mass transfer is a crucial factor in the design of biological processes particularly aerobic systems where dissolved oxygen in liquid phase can easily become a reaction limiting factor. Often the rate of gas–liquid mass transfer is empirically determined from the time profile of dissolved oxygen concentration in the system where information about bubble size and its distribution is neglected. However, a number of evidences have emphasized the significance of bubble properties in controlling the mass transfer in gas–liquid contacting systems. For bubble columns, bubble size was usually found to decrease with increasing gas input to the system, and therefore, high gas–liquid interfacial area was obtained at high gas throughput [1–5]. This was in contrast with a finding of Bochholz et al. [6], who investigated the relationship among bubble diameter, gas holdup and volumetric mass transfer coefficient. They reported that bubble coalescence become more significant at higher rate of gas throughput in a pilot scale bubble column.

Bubble size was reported to decrease with axial distance along the column height [7,8]. Types of gas sparger were also found to have remarkable effect on bubble size distribution in bubble columns. Hebrard et al. [4] reported that the use of perforated gas spargers led to a larger bubble size and broader bubble size distribution than those obtained from porous or membrane spargers. Meanwhile, Camarasa et al. [9] showed that various types of spargers provided different bubble size distributions resulting in different gas holdup profiles in bubble columns.

In airlift contactors (ALCs), the volumetric mass transfer rate was often reported as a function of operating and design parameters. Only a few investigations have looked through bubble size distribution in the ALC. Miyahara et al. [10] stated that bubble size distribution in the ALC exhibited the log-normal form which indicated that there existed a larger portion of small (3–4 mm), rather than large (4–6 mm), gas bubbles in the system. Miyahara and Hayashino [11] demonstrated further that this distribution varied with gas throughput such that bubble diameter became larger and size distributions became broader with an increase in superficial gas velocity (u_{sg}). These results were attributed to the predominance of bubble coalescence at low u_{sg} ($0.003 < u_{sg} < 0.03$ m/s). In contrast, Colella et al. [8] proposed some mechanisms for bubble coalescence and breakage in the annulus sparged ALC and concluded that higher superficial gas velocity tended to break bubbles into smaller size rather than to coalesce into bigger ones. The relative frequency of small bubble was found to be a function of u_{sg} and axial distance from the sparger.

The investigation on the bubble size distribution in the ALC is still limited and, thus far, there has not been sufficient information on effects of design parameters on the

* Corresponding author. Tel.: +66-2-218-6870; fax: +66-2-218-6877.
E-mail address: prasert.p@chula.ac.th (P. Pavasant).

1385-8947/02/$ – see front matter
PII: S1385-8947(02)00122-5

Nomenclature

a_L	specific gas–liquid interfacial area based on liquid volume (m^2/m^3)
A_d	downcomer cross-sectional area (m^2)
A_r	riser cross-sectional area (m^2)
d_B	equivalent size of the bubble (m)
d_{Bs}	Sauter mean bubble diameter (m)
D_l	diffusivity (m^2/s)
$f(d_B)$	relative frequency of bubble size, d_B
H_D	dispersion height (m)
H_L	unaerated liquid height (m)
g	gravitation acceleration (m^2/s)
Gr	Grashof number ($d_{Bs}^3 \rho_l \Delta\rho g/\mu_l^2$)
H_{dt}	draft tube height (m)
k_L	mass transfer coefficient based on liquid phase (m/s)
$k_L a_L$	overall volumetric mass transfer coefficient (s^{-1})
Re	Reynolds number ($d_{Bs} v_s \rho_l/\mu_l$)
Sh	Sherwood number ($k_L d_{Bs}/D_l$)
u_∞	terminal rise velocity of bubbles (m/s)
u_L	superficial liquid velocity (m/s)
u_{sg}	superficial gas velocity (m/s)
v_s	slip velocity (m/s)
x	axial distance from the sparger (m)
Δh	distance between pressure measurement points (m)
ΔP	hydrostatic pressure difference between two measuring points (N/m^2)

Greek symbols

δ	standard deviation (m)
$\varepsilon_{g,o}$	overall gas holdup
$\varepsilon_{g,d}$	downcomer gas holdup
$\varepsilon_{g,r}$	riser gas holdup
μ_l	viscosity (kg/(m s))
ρ_l	liquid density (kg/m^3)
ρ_g	gas density (kg/m^3)
σ	surface tension (N/m)

Subscripts

r	riser
d	downcomer
T	total

size distribution of bubbles. This work, hence, intends to examine the bubble size and its size distribution in the annulus sparged concentric ALC. The dependence of bubble characteristics on the contactor design and operating conditions is comprehensively investigated. This work also scrutinizes the effects of bubble sizes on the overall gas–liquid mass transfer ($k_L a_L$) in ALCs. An empirical model for the prediction of the mass transfer coefficient will be proposed.

2. Experimental

2.1. Apparatus

A schematic diagram of experimental setup for this work is shown in Fig. 1. Experiments were carried out in a transparent cylindrical column with a height of 1.2 m and a diameter of 0.137 m. The column was equipped with pressure taps at distance of every 0.1 m along the contactor height for the measurement of pressure drop, ΔP which was used to determine the riser gas holdup, $\varepsilon_{g,r}$. A draft tube with a height of 1 m was inserted into the column where a clearance between the column base and the end of the draft tube was fixed at 5 cm. The ratio between cross-sectional areas of downcomer and riser was altered by changing the draft tube diameter of which the dimension is provided in Table 1. The unaerated water level was controlled at 3 cm above the top of these draft tubes. Experiments were operated in a semi-batch operation where a continuous air flow was supplied through a perforated ring sparger into the water-filled column. Air flow rate was controlled by a calibrated rotameter to give a range of superficial gas velocity, u_{sg} from 0.0059 to 0.0737 m/s. The air spargers employed here were perforated rings made of a 0.8 cm diameter PVC tubing with 1 mm orifices. The sparger was located at the base of annular section. Three spargers with different orifice numbers, i.e. 5, 14 and 30, were employed to investigate the effect of gas sparger on bubble size, d_B. Table 2 summarizes the detail on specifications of each contactor employed in this work.

2.2. Measurements

2.2.1. Bubble size distribution

The measurements of bubble size and its distribution were performed in the riser using a photographic technique. The sizes of not less than 200 bubbles were measured for each experiment. At steady-state, images of bubbles

Table 1
Dimensions of draft tubes

Draft tube	Internal diameter (m)	External diameter (m)	A_d/A_r
1	0.093	0.10	1
2	0.0735	0.079	0.43
3	0.034	0.04	0.067

Table 2
Specification of ALC used in this work

Key	A_d/A_r	Number of orifices on sparger
ALC-1	0.067	14
ALC-2	0.43	14
ALC-3	1	14
ALC-4	1	30
ALC-5	1	5

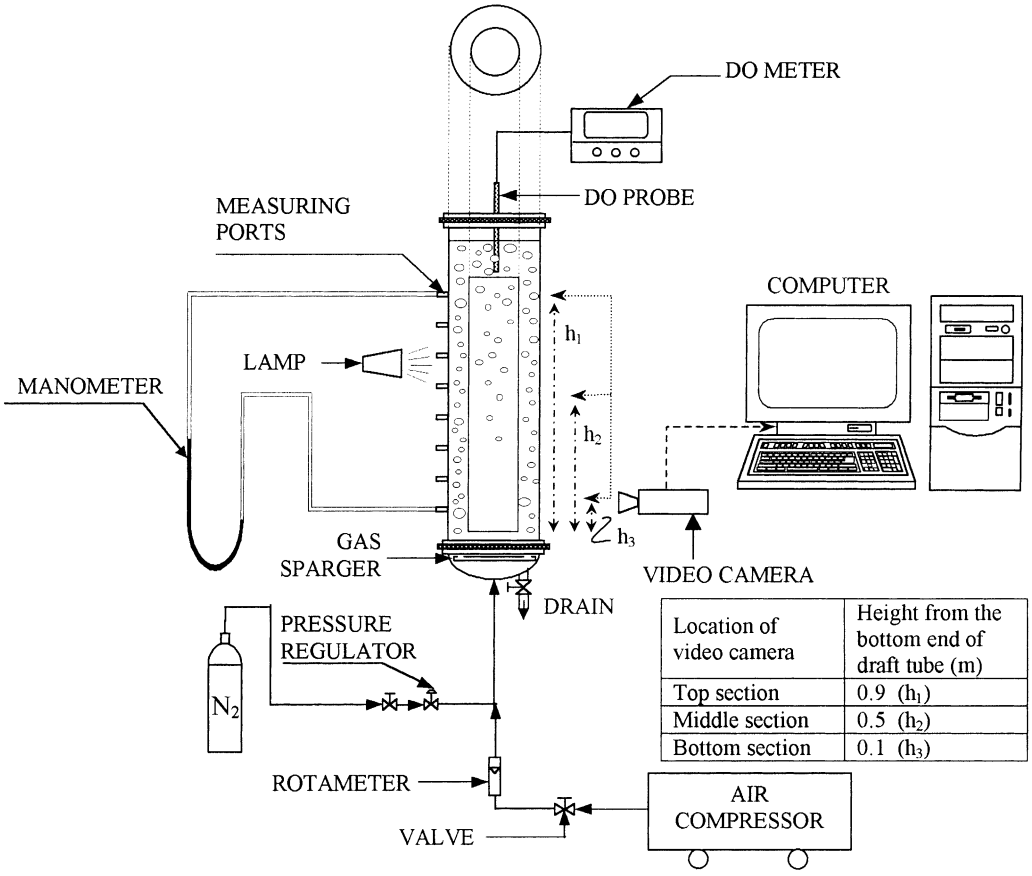

Fig. 1. A schematic diagram of experimental setup employed in this work.

were photographed using a digital video camera (SONY DCR-TRV20E) at three different heights (x): 0.1 m (bottom section), 0.5 m (middle section) and 0.9 m (top section) from the base of the draft tube. The correction to real size was based on the scale attached to the draft tube, which was at the same focal distance as the measured bubbles. In fact, the focus was adjusted on the scale and only the well-focalized bubbles were measured. For ellipsoidal bubbles, the major and minor axes of bubble images were measured. The equivalent size of the bubble (d_B), representing the diameter of a sphere whose volume is equal to that of the bubble, can then be calculated [4,5].

2.2.2. Determination of hydrodynamic and mass transfer behavior of ALCs

2.2.2.1. Gas holdup. The overall gas holdup, $\varepsilon_{g,o}$ was determined by the volume expansion method. The unaerated and aerated liquid heights were measured and $\varepsilon_{g,o}$ was then calculated from the following:

$$\varepsilon_{g,o} = \frac{H_D - H_L}{H_D} \quad (1)$$

The riser gas holdup, $\varepsilon_{g,r}$ was estimated by measuring the pressure difference, ΔP between the two pressure taps located along the height of the column, Δh where

$$\varepsilon_{g,r} = 1 - \frac{\Delta P}{\rho_l g \Delta h} \quad (2)$$

It was assumed that gas holdup in the top section was approximately equal to that in the riser, and therefore, the downcomer gas holdup, $\varepsilon_{g,d}$ can be computed from:

$$\varepsilon_{g,d} = \frac{\varepsilon_{g,o} H_D (A_d + A_r) + (H_{dt} A_d - H_D (A_d + A_r)) \varepsilon_{g,r}}{H_{dt} A_d} \quad (3)$$

2.2.2.2. Liquid velocity. Liquid velocities both in the riser and downcomer were measured using the color tracer technique. The pressure taps were employed as injection points of the color tracer and the travelling time of color tracer between the two points in the contactor was measured for the calculation of liquid velocity.

2.2.2.3. Gas–liquid mass transfer coefficient. The overall volumetric mass transfer coefficient ($k_L a$) was determined by the dynamic method [12–15]. A dissolved oxygen meter (Jenway 9300) was used to record the changes in concentration of O_2 in a batch of water that had previously been freed of O_2 by bubbling through with N_2.

3. Results and discussion

3.1. Error compensation in photographic technique

The measurement of bubble diameter in this study was taken along axial direction. The radial distribution of bubble size was not observed as the annulus of the employed ALCs had a rather small cross-sectional area where the distance between the inner and outer columns was only 1.85–4.85 cm, which was approximately in the same order of magnitude with the bubble. This did not allow precise measurement of bubble sizes along the radial direction. The measured sizes of bubbles were subject to error due to the curvature of the column surface. To account for this error, an object with a known size was placed along radial direction in the column and its picture was taken for size compensation. The error was then calculated and used as a correction factor for subsequent measurement. Note that the error due to the curvature of the column surface was approximately ±15%. Fig. 2 is an example of photographs of bubbles obtained from this measurement technique.

3.2. Bubble size distribution as a function of superficial gas velocity

Fig. 3 shows that there was a wide range of bubble sizes in ALC-3 and the distribution of bubble size varied with superficial gas velocity (u_{sg}). Note that, due to the equipment limitation, the ALC could only be operated with a limited level of u_{sg}. The maximum u_{sg} for each ALC depends markedly on the ratio between the downcomer and riser cross-sectional areas (A_d/A_r) such that ALC with higher A_d/A_r could be operated with higher level of u_{sg}. The maximum u_{sg} for ALCs with A_d/A_r of 0.067, 0.43 and 1 were 0.0415, 0.0516 and 0.0737 m/s, respectively.

Fig. 3 illustrates that, at a low level of u_{sg} (<0.01 m/s), the bubble size distribution at the bottom section of the ALC were narrow (standard deviations δ of 1.1–2.3 mm) and followed the normal distribution type (results from ALC-1, ALC-2, ALC-4 and ALC-5 showed similar trends but were not displayed here for a brevity purpose). It can be seen from the figure that a majority of gas bubbles in the system at this condition had a diameter of 6.0–8.0 mm. However, the same figure illustrated that, at low u_{sg}, the distributions of bubble sizes at the middle and top sections of the ALC deviated significantly from the normal type. This variation of bubble distribution along the column height will be explained in the next section. For cases where u_{sg} was between 0.02 and 0.04 m/s, there appeared two or more distinct peaks in the distribution curve which implied that at least two dominant sizes of bubbles were present in the system. For instance, Fig. 3 demonstrates that, at u_{sg} of 0.0296 m/s, there existed a group of relatively large bubbles with diameters of 7.0–8.0 mm and the other group of smaller bubbles with diameters of 4.0–6.0 mm. Due to the presence of various dominant groups of bubble sizes, the distribution of bubble size became broader (δ of 1.4–2.7 mm), and the bimodal or multimodal distribution was best to describe the size distribution in this range of u_{sg}. At high u_{sg} (>0.05 m/s), large bubbles disappeared and smaller bubbles with diameter of 3.0–6.0 mm dominated the system. The bubble size distribution in this range of u_{sg} had a standard deviation of 1.2–3.6 mm and was well described by an asymmetric log-normal distribution curve. This finding reveals clearly that an increase in u_{sg} reduced the number of large bubbles and increased the number of smaller size bubbles: the results which were in good agreement with those reported by Mahajan and Mahajan [3].

This shift in bubble size from large at low range of u_{sg} to small at high range of u_{sg} indicated that there was bubble breakage taken place in the system. According to Prince and Blanch [16], bubble breakage was caused by energy from turbulent eddies of appropriate size obtained from interactions between bubbles. Literature has shown that an increase in u_{sg} led to high liquid velocity [17–19] and this might be responsible for the enhancement of turbulent intensity. In other words, higher u_{sg} resulted in greater turbulent intensity which caused more bubble breakage and led to a reduction in average bubble size as illustrated in Fig. 4. However, further increase in u_{sg} (>0.05 m/s) was no longer observed to have significant effect on bubble size. This may be due to the stability of small bubble against the breakage mechanism at high u_{sg} [20,21].

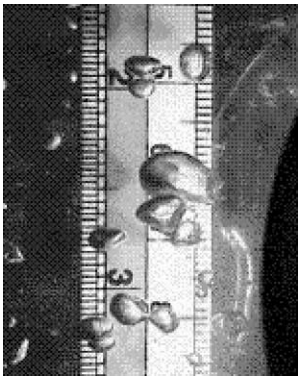

Fig. 2. An example of photograph of bubbles at the middle section of ALC-5 at u_{sg} = 0.0296 m/s.

3.3. Axial variation of bubble size distribution

The bubble size was found to depend significantly on the axial location in the ALC. Fig. 4 shows that the average bubble size at the base of the contactor was found to be the largest and it continued to decrease as bubbles moved along contactor height. This implied that there existed a breakage mechanism of bubbles. This finding was in good agreement with some reported measurements in bubble columns [7,8] and in the ALC [11].

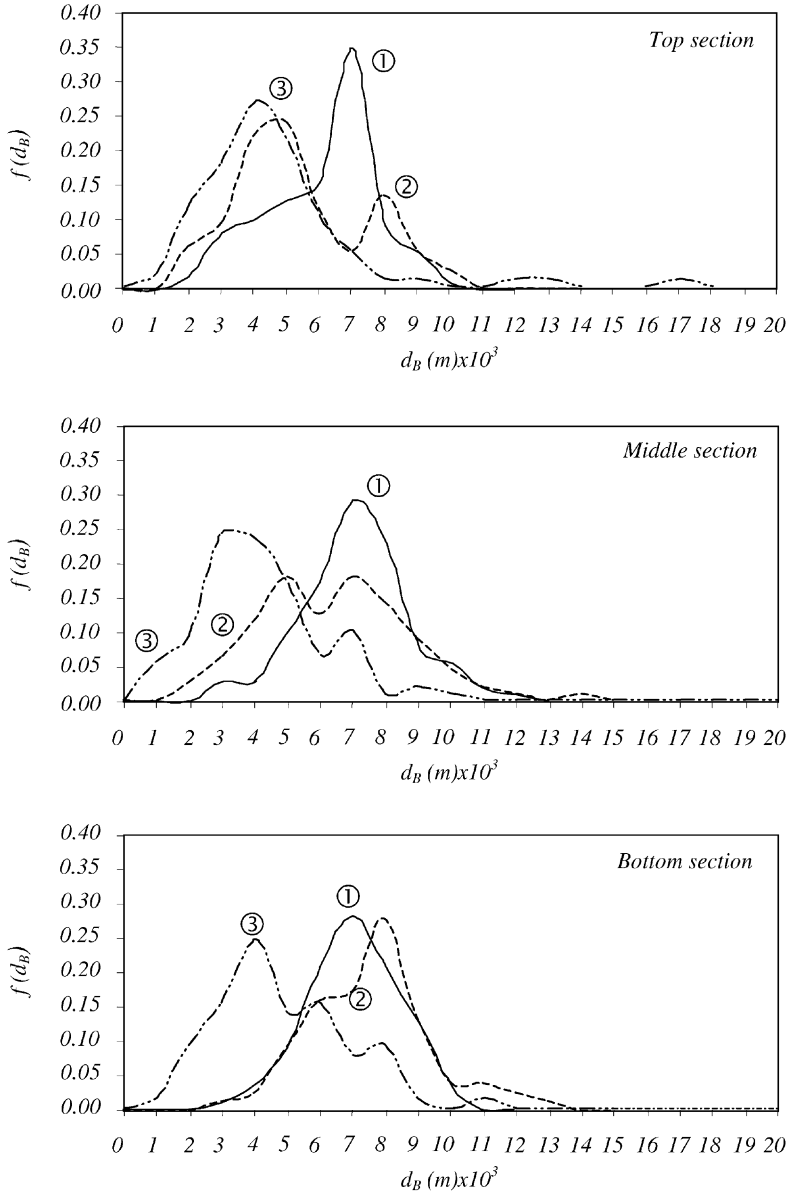

Fig. 3. Frequency distribution of bubble sizes in ALC-3 at various u_{sg}: (1) $u_{sg} = 0.0085$ m/s, (2) $u_{sg} = 0.0296$ m/s and (3) $u_{sg} = 0.0593$ m/s.

In view of bubble size distribution, there was a slight difference in terms of transition of bubble size distributions (unimodal to bimodal or multimodal and to log-normal types) along the column height. In other words, changes in the types of distribution occurred at different levels of u_{sg}. For instance, at the bottom section of ALC-3 in Fig. 3, the transition from unimodal to bimodal or multimodal distributions occurred at u_{sg} of as high as 0.0296 m/s, whereas this transition at the top part took place at u_{sg} of as small as 0.0085 m/s. This result was attributed to the bubble breakage along the column height which resulted in a high proportion of small bubbles at the higher section where the distribution curve tended to shift faster towards the small size region.

3.4. Bubble size distribution and the ratio between riser and downcomer cross-sectional areas

To investigate the effect of the ratio between the downcomer and riser cross-sectional areas (A_d/A_r), the experiment was conducted in the system with three different A_d/A_r, i.e. 0.067 (ALC-1), 0.43 (ALC-2), and 1 (ALC-3). Fig. 5 summarizes the results from these experiments where it was found that, at low gas throughput ($u_{sg} < 0.0296$ m/s), A_d/A_r did not significantly affect bubble sizes. However, A_d/A_r tended to have an influence on bubble size and its size distribution at high gas throughput where the ALC with A_d/A_r of 0.43 (ALC-2) was found to give the smallest bubble size.

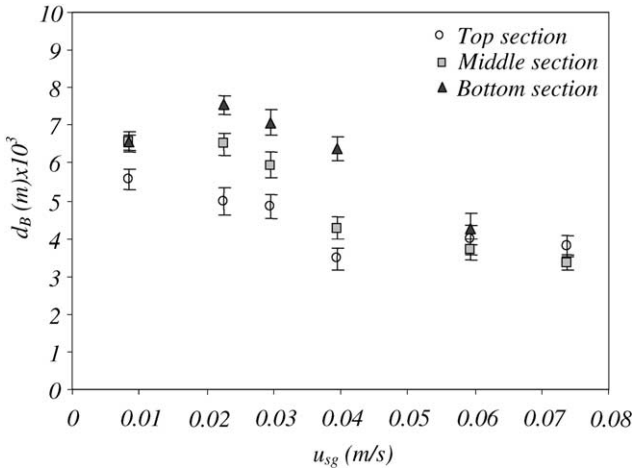

Fig. 4. Relationship between average bubble diameter, d_B and superficial gas velocity, u_{sg} along axial location in ALC-3.

3.5. Effect of gas sparger on bubble size distribution

The effect of gas sparger on the distribution of bubble sizes in ALCs is illustrated in Fig. 6. The average bubble size tended to increase with increasing orifice number of sparger. Bubbles from the sparger with 30 orifices seemed to coalesce quickly once they left the orifices. This was because each orifice was close to each other which facilitated the coalescence between new-born bubbles. In this context, bubbles from the sparger with five orifices should be the smallest in size, which was true in most cases but not at the bottom section where average bubble size was found to be much larger than at other sections. It was also found that the distribution of bubble size at this situation (five orifice sparger) was much wider than other cases. This might be due to the high pressure in the sparger with less number of orifices which caused new-born bubbles to be very large in size and these bubbles broke rapidly after leaving the orifice.

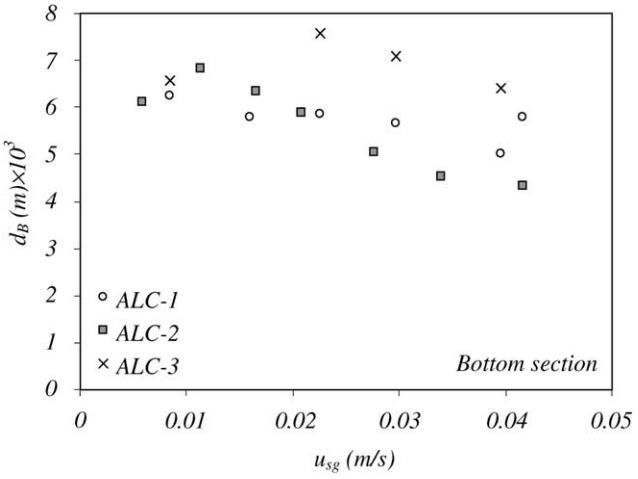

Fig. 5. Relationship between average bubble diameter, d_B and cross-sectional area ratio between the downcomer and riser, A_d/A_r.

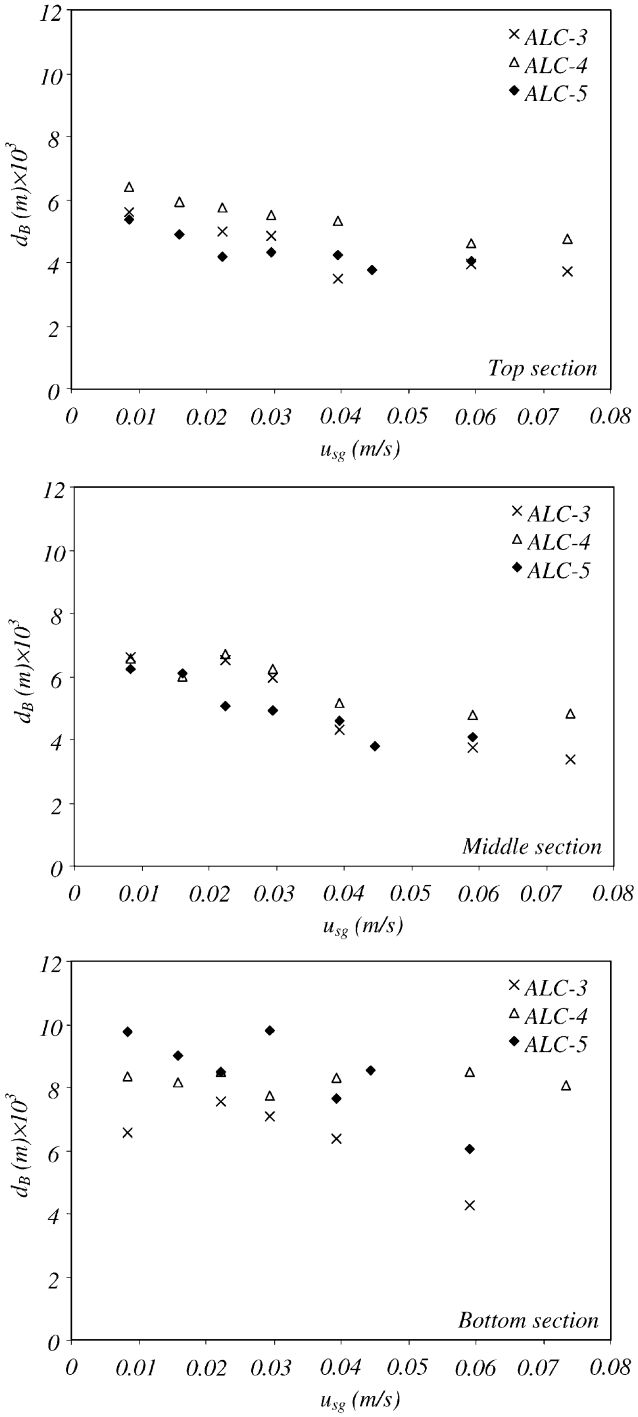

Fig. 6. Relationship between average bubble diameter, d_B and orifice number, n along axial location.

3.6. Overall volumetric mass transfer coefficient ($k_L a_L$) in airlift contactors

The relationships between the overall volumetric mass transfer coefficient, $k_L a_L$ in the ALC with various parameters are shown in Fig. 7. This demonstrates that $k_L a_L$ increased with u_{sg} but decreased with increasing A_d/A_r, whilst

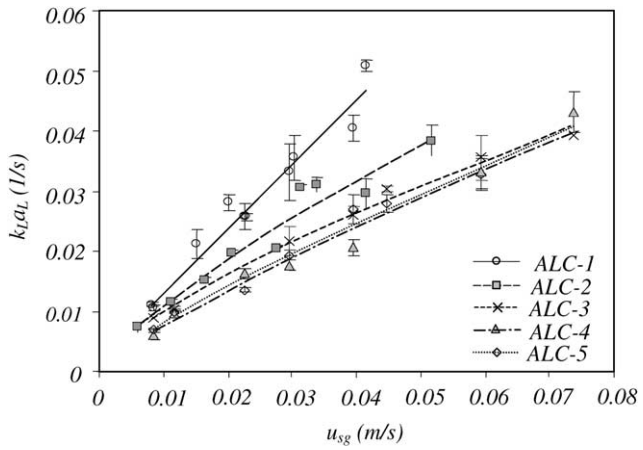

Fig. 7. Relationship between experimental data of overall volumetric mass transfer coefficient, $(k_L a_L)_T$ and superficial gas velocity, u_{sg}.

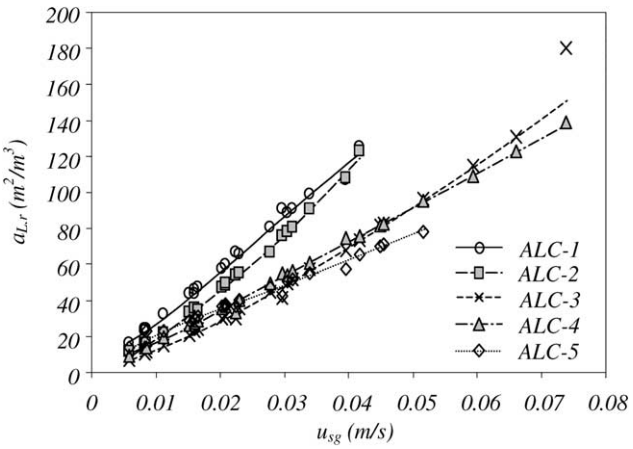

Fig. 8. Relationship between specific interfacial area in riser, $a_{L,r}$ and superficial gas velocity, u_{sg}.

the influence of number of holes in sparger on $k_L a_L$ was negligible in the range of condition employed in this study. The following sub-sections investigate the influence of these parameters on $k_L a_L$ in detail.

3.7. Determination of overall gas–liquid mass transfer coefficient ($k_L a_L$)

With information on bubble size distribution, it was possible to estimate $k_L a_L$ in terms of k_L and a_L separately. The specific interfacial area, a_L is defined according to Eq. (4) where bubbles are assumed to be spherical with an average diameter of d_B

$$a_L = \frac{6\varepsilon_g}{(1-\varepsilon_g)d_B} \tag{4}$$

Gas holdups, ε_g were directly measured from the experiments, whereas the bubble diameter, d_B employed in the determination of a_L in Eq. (4) is usually reported as "Sauter mean diameter, d_{Bs}" or surface volume mean diameter which can be calculated from

$$d_{Bs} = \frac{\sum n_i d_{B,i}^3}{\sum n_i d_{B,i}^2} \tag{5}$$

where n_i is the number of bubbles with diameter $d_{B,i}$. As reported in previous sections, the bubble size in the riser, $d_{B,r}$ was not uniform along the axial direction. For each experimental condition, specific interfacial area in riser, $a_{L,r}$ was, therefore, calculated using information on bubble size distribution along the column height together with riser gas holdup, $\varepsilon_{g,r}$ which was assumed to be uniform in both radial and axial directions as follows:

$$a_{L,r} = \frac{1}{H_{dt}} \int_{x_r=0}^{x_r=H_{dt}} a_{L,x_r}\, dx_r = \frac{1}{H_{dt}} \frac{6\varepsilon_{g,r}}{(1-\varepsilon_{g,r})} \int_{x_r=0}^{x_r=H_{dt}} \frac{1}{d_{Bs,x_r}}\, dx_r \tag{6}$$

It is worth noting here that the integration in Eq. (6) was performed by dividing the ALC into three sections: bottom, middle and top, and all bubbles in each section were assumed to have the same size. The relationships between $a_{L,r}$ and u_{sg} for the various ALCs in this work are shown in Fig. 8.

Due to the limitation of the photographic technique, the direct observation of bubble size in downcomer was not possible. The average bubble size in downcomer, $d_{B,d}$ was estimated from experimental data on liquid velocity in downcomer, $u_{L,d}$ using the Levich equation [22], Eq. (7). The $d_{B,d}$ was then assumed to be equal to the size of bubble with a terminal velocity equal to the liquid velocity in downcomer.

According to Levich [22]:

$$d_{B,d} = \frac{1.8}{g}\left(\frac{u_{L,d}}{2}\right)^2 \tag{7}$$

It was assumed further that there was no variation of bubble size along the radial and axial directions in downcomer. Therefore,

$$d_{Bs,d} = d_{B,d} \tag{8}$$

The $a_{L,d}$ was calculated from the substitution of $d_{Bs,d}$ from Eq. (8) together with $\varepsilon_{g,d}$ (from experiment) into Eq. (4). The circulating velocities (in terms of downcomer liquid velocity) in the ALCs were measured and are displayed in Fig. 9.

The mass transfer coefficient, k_L was commonly reported as a function of properties of liquid and bubble size [23–26]. Several empirical and theoretical correlations for the determination of mass transfer coefficient, k_L for various systems are given and summarized in Skelland [27], Treybal [28], Welty et al. [29] and Stanley [30]. Eq. (9) is often employed as an initial point for the establishment of k_L correlation.

$$Sh = a + \underbrace{b\,Gr^c}_{\text{free rise bubble}} + \overbrace{d\,Re^e}^{\text{forced convection}} \tag{9}$$

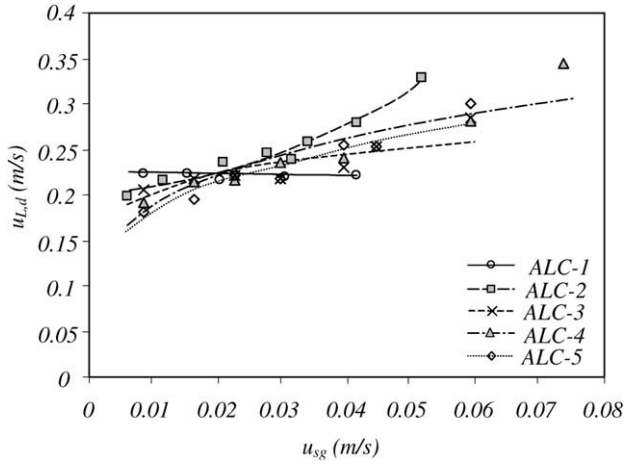

Fig. 9. Relationship between superficial liquid velocity in downcomer, $u_{L,d}$ and superficial gas velocity, u_{sg}.

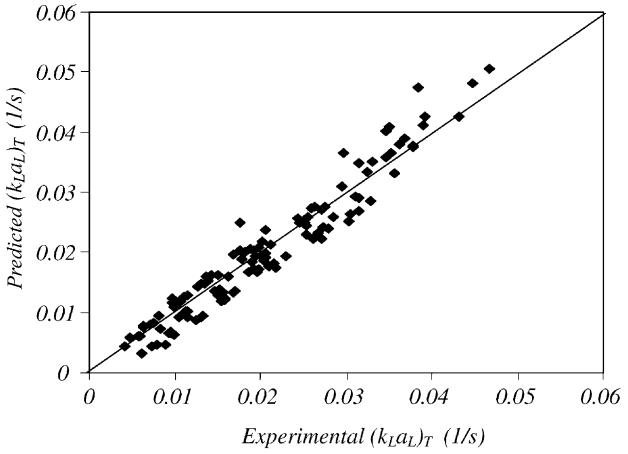

Fig. 10. Comparison of $(k_La_L)_T$ estimated by Eq. (15) with values observed in this work.

Generally, Grashof number, *Gr* represents mass transfer by natural convection or free rise velocity whilst Reynolds number, *Re* is for mass transfer by forced convection. The parameters *a–e* in Eq. (9) are determined experimentally. Eq. (9) requires that slip velocity, v_s and Sauter bubble diameter, d_{Bs} are known in a priori.

The Sauter mean bubble diameter in the riser, $d_{Bs,r}$ was calculated from the information on $d_{Bs,r}$ along the column height as follows:

$$d_{Bs,r} = \frac{1}{H_{dt}} \int_{x_r=0}^{x_r=H_{dt}} d_{Bs,x_r}\, d\, x_r \tag{10}$$

The Sauter bubble diameter in downcomer, $d_{Bs,d}$ was calculated from Eq. (8). The slip velocity was also calculated separately in each section of the ALC. The slip velocity in the riser, $v_{s,r}$ is a function of the terminal rise velocity of a single bubble, u_∞ which is modified to account for hindering effects from neighboring bubbles in the riser [31–35] such that:

$$v_{s,r} = \frac{u_\infty}{(1-\varepsilon_{g,r})} \tag{11}$$

The terminal bubble rise velocity, u_∞ can be calculated using the correlation developed by Jamialahmadi et al. [36]:

$$u_\infty = \frac{(1/18)(\rho_l - \rho_g/\mu_l) g d_{Bs}^2 (3\mu_l + 3\mu_g/2\mu_l + 3\mu_g)\sqrt{(2\sigma/d_{Bs}(\rho_l+\rho_g)) + g d_{Bs}/2}}{\sqrt{[(1/18)(\rho_l - \rho_g/\mu_l) g d_{Bs}^2 (3\mu_l + 3\mu_g/2\mu_l + 3\mu_g)]^2 + 2\sigma/d_{Bs}(\rho_l+\rho_g) + g d_{Bs}/2}} \tag{12}$$

It was assumed here that bubbles in the downcomer had terminal rise velocity equal to liquid velocity and bubble size was uniform along the column height. The slip velocity can, therefore, be estimated from the downcomer liquid velocity:

$$v_{s,d} = u_{L,d} \tag{13}$$

Substituting $d_{Bs,r}$ in Eq. (10) and $n_{s,r}$ in Eq. (11) into Eq. (9) leads to the correlation for the determination of $k_{L,r}$ where the same procedure can be applied for $d_{Bs,d}$ (Eq. (8)) and $v_{s,d}$ (Eq. (13)) to yield the correlation for $k_{L,d}$.

3.8. Comparison between k_La_L from experiment and prediction

The mass transfer rate for the entire contactor was expressed in terms of the overall volumetric mass transfer coefficient $(k_La_L)_T$ and this can be calculated from the sum of the mass transfer rates in riser and downcomer as follows:

$$(k_La_L)_T = \frac{(k_La_L)_r V_{L,r} + (k_La_L)_d V_{L,d}}{V_{L,T}} \tag{14}$$

where $V_{L,r}$ is the volume of liquid in riser, $V_{L,d}$ the volume of liquid in downcomer and $V_{L,T}$ the total volume of liquid. The $(k_La_L)_r$ and $(k_La_L)_d$ in this equation are obtained from the product between $k_{L,r}$ and $a_{L,r}$, and $k_{L,d}$ and $a_{L,d}$, respectively. Fig. 10 illustrates the comparison between the predicted k_La_L from Eq. (15) and the experimental value which shows that there was a good agreement between the two when parameters *a–e* in Eq. (9) were equal to 0.5, 1.07, 0.469, 0 and 0, respectively (note that these parameter were obtained from the solver function in the MS Excel 97 where the objective was a minimal error between experimental and simulation data). Eq. (9) now becomes:

$$Sh = 0.5 + 1.07\, Gr^{0.469} \tag{15}$$

Eq. (15) indicates that when $d = 0$, *Re* disappears, which means that forced convection has no effect on the mass transfer. This finding reveals that the mass transfer in the ALC employed in this work depended primarily on the natural convection, and not the force convection.

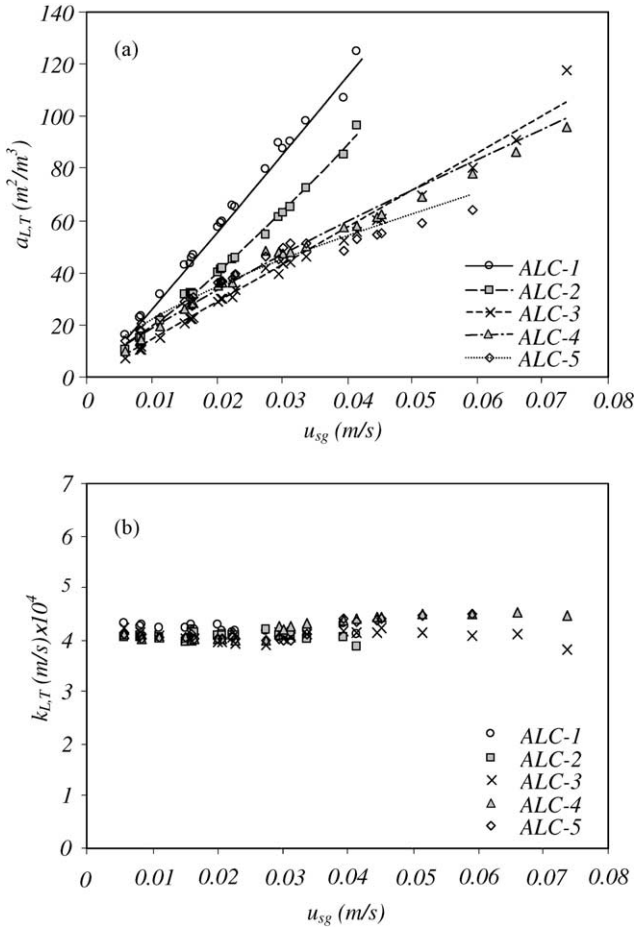

Fig. 11. Effects of superficial gas velocity, u_{sg} on (a) overall specific interfacial area, $a_{L,T}$ and (b) overall mass transfer coefficient, $k_{L,T}$.

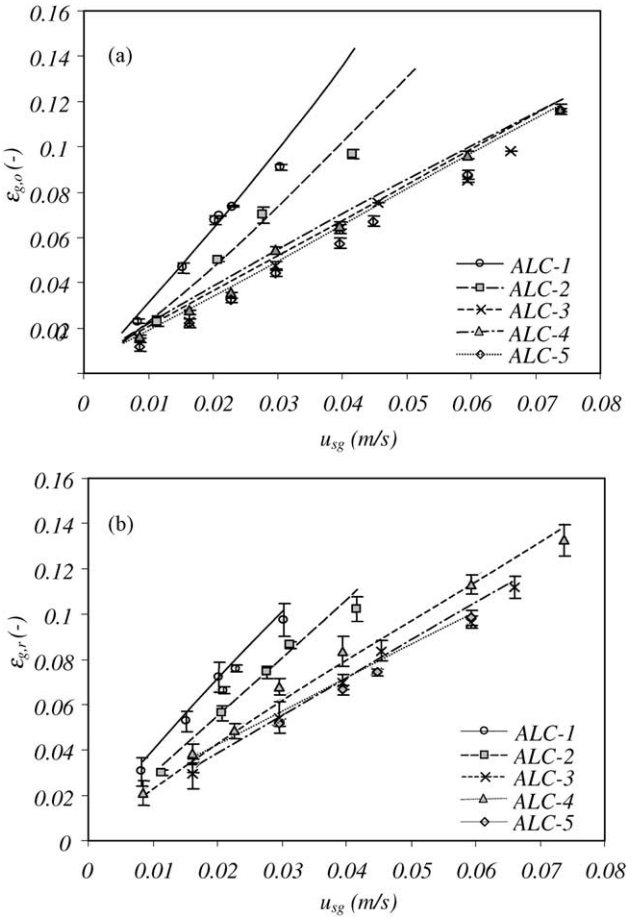

Fig. 12. Effects of superficial gas velocity, u_{sg} on (a) overall gas holdup, $\varepsilon_{g,o}$ and (b) riser gas holdup, $\varepsilon_{g,r}$.

3.9. Evaluation of $k_L a_L$ in the ALC

Fig. 11 demonstrates the variations of overall k_L ($k_{L,T}$) and a_L ($a_{L,T}$) with u_{sg} in all of the ALCs employed in this work which reveals that a_L varied almost linearly with u_{sg} whilst k_L only slightly changed with u_{sg}. Therefore, it should be reasonable to conclude that the increase in a_L with u_{sg} in the ALC was the main factor responsible for the increase in $k_L a_L$ (see Fig. 7). This increase in a_L was attributed to the increase in the overall gas holdup (Fig. 12) and the decrease in the bubble size with the gas throughput (Fig. 4). Fig. 11 demonstrates that the change in bubble size with u_{sg} did not cause a drastic deviation in the value of k_L, and therefore, changes in k_L only slightly affect the overall volumetric mass transfer coefficient.

Fig. 11 also describes the effects of A_d/A_r on k_L and a_L (ALC-1, ALC-2 and ALC-3). The ALC with larger A_d/A_r rendered the liquid circulating velocity to be faster (Fig. 9) and this reduced gas holdup in the system (Fig. 12). Although the bubble size in a large A_d/A_r ALC was found to be smaller than ALC with small A_d/A_r (at high u_{sg}), its effect on the enhancement of specific mass transfer area was overwhelmed by the reduction in gas holdup. This resulted in a smaller a_L in ALCs with high A_d/A_r. In contrast, the increase in A_d/A_r did not seem to have significant influence on the mass transfer coefficient, k_L. Hence, the decrease in $k_L a_L$ with A_d/A_r in Fig. 7 was mainly due to the decrease in a_L.

Fig. 7 indicates that the influence of number of orifices in the sparger on $k_L a_L$ was negligible in the range of conditions used in this study. This was verified by the analysis in this section and the results in Fig. 11 (ALC-3, ALC-4 and ALC-5) revealed that both k_L and a_L were found not to be influenced by the number of orifices in the sparger. As a_L varies inversely with the bubble size and since a larger number of orifices resulted in a larger bubble size, the ALC with this type of sparger should have led to a system with a smaller a_L. However, the results clearly illustrate that this was not the case and a_L in ALC-4 (30 orifice sparger) was found to be similar to a_L in ALC-5 (five orifice sparger). This was because the effect of the larger bubble size on the specific area was compensated by the effect of larger overall gas holdup in the system.

4. Conclusion

This work illustrated the effect of various design and operating parameters on bubble size distribution in the ALC. The results suggested that, with a proper design of the ALC, one might, to some extent, be able to control the bubble behavior in the system. A technique for the estimation of specific interfacial area based on the information on bubble size distribution was then proposed along with the development of an empirical correlation for the prediction of mass transfer coefficient. It was shown that a thorough investigation on the effect of various parameters on the rate of gas–liquid mass transfer could be performed with additional data on bubble size distribution. This is particularly useful for further development and control of the ALC for applications where gas–liquid mass transfer is important.

Acknowledgements

The authors wish to acknowledge the Thailand Research Fund, Asahi Glass Foundation and TRF Senior Scholar Project (W. Tanthapanichakoon) for their financial supports.

References

[1] J.O. Hinze, Fundamentals of the hydrodynamic mechanism of splitting in dispersion processes, AIChE J. 33 (1955) 289–295.
[2] K. Akita, F. Yoshida, Bubble size, interfacial area and liquid phase mass transfer coefficient in bubble columns, Ind. Eng. Chem. Process Des. Dev. 13 (1974) 84–91.
[3] S.P. Mahajan, G.S.R. Mahajan, Size, size distribution, size distribution and interfacial area for gas–liquid dispersions formed on perforated plates, Ind. J. Tech. 13 (1975) 541–547.
[4] G. Hebrard, D. Bastoul, M. Roustan, Influence of the gas sparger on the hydrodynamic behavior of bubble columns, Trans. Inst. Chem. Eng. 74 (1996) 406–414.
[5] A. Couvert, M. Roustan, P. Chatellier, Two-phase hydrodynamic study of a rectangular airlift loop reactor with an internal baffle, Chem. Eng. Sci. 54 (1999) 5245–5252.
[6] H. Bochholz, R. Buchholz, J. Lücke, K. Schugerl, Bubble swarm behavior and gas absorption in non-Newtonian fluids in sparged columns, Chem. Eng. Sci. 33 (1978) 1061–1070.
[7] T. Otake, S. Tone, K. Nakao, Y. Mitsuhashi, Coalescence and breakup of bubbles in liquids, Chem. Eng. Sci. 32 (1977) 377–383.
[8] D. Colella, D. Vinci, R. Bagatin, M. Masi, E.A. Bakr, A study on coalescence and breakage mechanisms in three different bubble columns, Chem. Eng. Sci. 54 (1999) 4767–4777.
[9] E. Camarasa, C. Vial, S. Poncin, G. Wild, N. Midoux, J. Bouillard, Influence of coalescence behavior of the liquid and of gas sparging on hydrodynamics and bubble characteristics in a bubble column, Chem. Eng. Proc. 38 (1999) 329–344.
[10] T. Miyahara, M. Hamaguchi, Y. Sukeda, T. Takahashi, Size of bubbles and liquid circulation in a bubble column with a draft tube and sieve plate, Can. J. Chem. Eng. 64 (1986) 718–725.
[11] T. Miyahara, T. Hayashino, Size of bubbles generated from perforated plates in a non-Newtonian liquids, J. Chem. Eng. Jpn. 28 (1995) 596–601.
[12] Y. Chisti, M. Moo-Young, Hydrodynamics and oxygen mass transfer in a pneumatic bioreactor devices, Biotechnol. Bioeng. 31 (1988) 487–494.
[13] K. Koide, H. Sato, S. Iwamoto, Gas holdup and volumetric liquid-phase mass transfer coefficient in bubble column with draught tube and with gas dispersion into annulus, J. Chem. Eng. Jpn. 16 (5) (1983) 407–413.
[14] H.-L. Tung, C.-C. Tu, Y.-Y. Chang, W.-T. Wu, Bubble characteristics and mass transfer in an airlift reactor with multiple net draft tubes, Bioproc. Eng. 18 (1998) 323–328.
[15] M. Bouaifi, G. Hebrard, D. Bastoul, M. Roustan, A comparative study of gas hold-up, bubble size, interfacial area and mass transfer coefficients in stirred gas–liquid reactors and bubble columns, Chem. Eng. Proc. 40 (2001) 97–111.
[16] M.J. Prince, H.W. Blanch, Bubble coalescence and break-up in air-sparged bubble columns, AIChE J. 36 (1990) 1485–1499.
[17] R.A. Bello, C.W. Robinson, M. Moo-Young, Gas hold-up and overall volumetric oxygen transfer coefficient in airlift contactors, Biotechnol. Bioeng. 27 (1985) 369–381.
[18] M.Y. Chisti, Airlift Bioreactors, Elsevier, London, 1989.
[19] K.H. Choi, W.K. Lee, Circulation liquid velocity, gas holdup and volumetric oxygen transfer coefficient in external-loop airlift reactors, J. Chem. Tech. Biotech. 56 (1993) 51–58.
[20] Y. Kawase, M. Moo-Young, Mathematical Models for design of bioreactors: applications of Kolmogoroff's theory of isotropic turbulence, Chem. Eng. J. 43 (1990) B19–B41.
[21] R.P. Hesketh, A.W. Etchells, T.W.F. Russell, Bubble breakage in pipeline flow, Chem. Eng. Sci. 46 (1) (1991) 1–9.
[22] V.G. Levich, Physicochemical Hydrodynamics, Prentice-Hall, Englewood Cliffs, NJ, 1962.
[23] R. Higbie, Rate of absorption of a pure gas into a still liquid during short period of exposure, Trans. Am. Inst. Chem. Eng. 31 (1935) 365–389.
[24] P.H. Calderbank, M. Moo-Young, The continuous phase heat and mass transfer properties of dispersions, Chem. Eng. Sci. 16 (1961) 39.
[25] P.H. Calderbank, Mass transfer in fermentation equipment, in: N. Blakebrough (Ed.), Biochemical and Biological Engineering Science, Vol. 2, Academic Press, New York, 1967, pp. 102–180.
[26] J.E. Bailey, D.F. Ollis, Biochemical Engineering Fundamentals, McGraw-Hill, New York, 1977.
[27] A.H.P. Skelland, Diffusional Mass Transfer, Wiley, New York, 1974.
[28] R.E. Treybal, Mass Transfer Operations, McGraw-Hill, New York, 1980.
[29] J.R. Welty, C.E. Wicks, R.E. Wilson, Fundamentals of Momentum, Heat, and Mass Transfer, Wiley, New York, 1984.
[30] M. Stanley, An Introduction to Mass and Heat Transfer, Wiley, New York, 1998.
[31] J.F. Richardson, W.N. Zaki, Sedimentation and fluidization. Part I, Trans. Inst. Chem. Eng. 32 (1954) 35.
[32] G. Marrucci, Rising velocity of a swarm of spherical bubbles, Ind. Eng. Chem. Fundam. 4 (1965) 224–225.
[33] J.F. Davidson, D. Harrison, The behavior of a continuity bubbling fluidized bed, Chem. Eng. Sci. 21 (1966) 731.
[34] J.C.R. Turner, On bubble flow in liquids and fluidized beds, Chem. Eng. Sci. 21 (1966) 971.
[35] G.B. Wallis, One Dimensional Two-Phase Flow, McGraw-Hill, New York, 1969.
[36] M. Jamialahmadi, C. Branch, H. Müller-Steinhagen, Terminal bubble rise velocity in liquids, Trans. Inst. Chem. Eng. Part A 72 (1994) 119–122.